Development of a Ferromagnetic Enhanced Ambipolar Plasma Thruster

IEPC-2024-171

Presented at the 38th International Electric Propulsion Conference, Toulouse, France
June 23-28, 2024

Christoph Peter*, Oliver Neunzig† and Martin Tajmar‡
Technische Universität Dresden, Dresden, Germany

Due to the increasing popularity of small and nano satellites due to their cost efficiency and lower financial hurdle, especially for institutions, there is also a growing interest and incentive to develop miniaturized propulsion systems or to optimize propulsion concepts for small satellites. Another area of research that is gaining interest is air-breathing propulsion systems. They are expected to significantly extend the duration of missions in very low Earth orbit, thus enabling longer missions with short latency and high resolutions for Earth observation. The propulsion system presented here addresses both areas of interest.

The presented propulsion concept is a radio frequency thruster with a ferromagnetic enhanced antenna. The effect of the ferrite core is discussed based on thrust measurements. We also present a setup to measure the thrust of any electric propulsion system without the need to install it on the thrust balance. This was used for the thruster presented here to obtain sub-micro-Newton precision measurements on an existing compact high-precision thrust balance.

The cathodeless thruster can be operated with conventional propellants as well as with gas mixtures comparable to those found in the Earth's atmosphere. The use of other alternative propellants is also discussed, and a tank concept for solid propellants that sublimate at temperatures around 60°C is presented.

I. Introduction

Electric propulsion has been an established technology in space for some time, primarily because of its advantages in fuel efficiency. This is critical for small satellites, as the amount of propellant available limits their lifetime in orbit. Gridded ion thrusters and Hall thrusters, for example, are proven technologies for electric propulsion systems. However, these conventional thruster concepts require a cathode for operation, presenting a major drawback, as the latter increases system size and complexity. Cathodes also can not use oxygen-rich gas mixtures such as air for prolonged periods of time. This renders most of the conventional thruster concepts unsuitable as fully air-breathing propulsion. There are also other alternative propellants of high interest, especially to small satellites, because of their high storage density without a pressurized tank system and their cost effectiveness compared to noble gases such as xenon. But because these are often complex organic molecules, decomposition during plasma ignition leads to negative ions in addition to the usually positively charged ions. These carbon rich negative ions are accelerated to the anode and accumulate there over time. This eventually shortens the anode or clogs up the propellant feed. Consequently, many interesting alternative propellants can not be used with conventional electric propulsion systems. Additionally, scaling laws make it very difficult to miniaturize Hall effect thrusters, for example, as the power density in components continues to increase while the heat transfer decreases.

*Doctoral candidate, Institute of Aerospace Engineering, christoph.peter@tu-dresden.de
†Doctoral candidate, Institute of Aerospace Engineering, oliver.neunzig@tu-dresden.de
‡Institute Director and Head of Space Systems Chair, Institute of Aerospace Engineering, martin.tajmar@tu-dresden.de

Propulsion technologies to overcome these drawbacks are cathodeless thrusters. They accelerate the plasma with a magnetic nozzle. This ambipolar acceleration allows completely cathodeless operation, as the resulting plasma beam is quasi-neutral. The propulsion concept presented here employs this acceleration mechanism and uses radio-frequency (RF) power to ignite the plasma. With our design, which features a special antenna with a ferrite core, we want to address common drawbacks to improve efficiency and usability of RF at lower power levels, to improve the viability for small satellites.

RF thrusters are the most common representative of cathodeless thrusters, with numerous concepts and system being developed and presented over the past several years. Of particular significance are Helicon plasma thrusters (HPT), which employ a specialized antenna designed to stimulate additional modes, known as whistler modes, within the plasma in order to increase the attainable plasma density following theoretical models.[1–5] This is especially relevant for high power systems, where it becomes increasingly more difficult to couple electromagnetic power into the plasma due to its self-shielding at increasing densities. Sheehan et al. developed a miniaturized CubeSat Ambipolar Thruster, which features a Helicon antenna.[6,7] With a power target of only 50 W, they employ permanent magnets for the magnetic nozzle to reduce the required power for operation. Many high power designs feature solenoids instead, due to their preferable magnetic field topology and flexibility.

For small satellites however, only permanent magnets are really viable, as the power consumption of the solenoids often matches or surpasses that of the actual RF power system, greatly reducing the overall efficiency of the thruster. Rotating magnetic fields for acceleration like Furukawa et al.[8] used are also mainly targeted for higher power systems. Smirnov et al.[9] use a capacitive coupled plasma (CCP) discharge for their design instead of the more common inductively coupled plasma (ICP) source, which also include Helicon antennas. The capacitive mode is easier to ignite and has a lower power requirement, but also a lower resulting plasma density.[9] This is why most designs feature some sort of ICP as plasma source. Plasma density jumps have been observed between CCP and ICP, as well as ICP and Helicon operation mode.[5] Helicons however are only observed at input powers of a few hundred watts.[5,10,11] It is also important to note, when comparing different excitation modes, that different types of antennas are not equally efficient for different coupling modes. That Helicon antennas are seen as more efficient, even at lower input powers, might very well arise from comparisons made with the same antenna at different power targets, despite the fact that there are more efficient antennas for the ICP mode.[12] Helicons are also a resonance phenomenon, making them challenging to control, particularly in an electric thruster application far from a controlled laboratory setting and with varying mass-flows and propellant composition changes experienced by air-breathing electric propulsion systems.

The objective of the activity presented in this paper is to develop a cathodeless thruster with an RF antenna for a power target of 50 W to 200 W. To improve the coupling efficiency, a ferrite core is used to increase the inductance of the antenna at lower plasma densities and increase the magnetic field of the antenna to improve plasma generation.[12–16] A secondary goal is also to reduce the dependency on a active matching between the ignition and operation states of the thruster, as such a matching system introduces complexity and absorbs additional power, both being a premium on small satellites.

II. Approach

A. Design idea

The antenna system's core concept is to apply the operating principle mainly used in the past for RF discharge lamps to an electric thruster while incorporating an external magnetic field to create a magnetic nozzle. The use of RF discharge for lighting became feasible after advancements in RF power converter technology.[17] Various designs have been utilized in the past for lamps with a loop antenna and a dielectric-contained plasma. The work on this resulted in plasma sources with the highest efficiency of commercial plasma sources ever achieved from the Endura/Icetron lamp of over 98 %.[12,15] Figure 1 shows two different types of such plasma sources.

The ferrite core increases the inductance of the antenna and reduces the inductance jump after plasma ignition slightly compared to the same system without the ferrite core. Comparable sources are also utilized for industrial applications like material processing.[13–15] Electric thruster design have been published that integrate a ferrite core into the antenna system. The PEGASES thruster is a gridded ion thruster with a

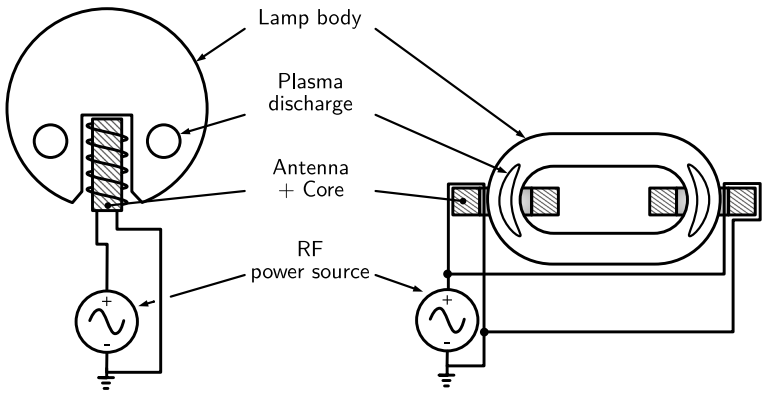

Figure 1: Schematics of two RF lamps with different types of antennas. Adapted from [17, p. 1], [18, p. 26], [15, p. 3]

planar antenna embedded in a ferrite body.[19–21] A similar conceptual design as been published by Rafalskyi et al.[22] Celik et al. use this concept in an RF cathode design.[23] A cathode for space application with a comparable design was presented by Godyak et al.[24] However, none of the designs use a ferromagnetic enhanced antenna in combination with a magnetic nozzle for acceleration. The design of the prototype and its iteration will be discussed in the following subsection.

B. Prototype design

1. Antenna core selection

The thruster design features a high-permeability core that encases the discharge chamber, similar to the schematic depicted on the right in Fig. 1. Different antenna configurations have been tested with the first prototype. In the current design iteration, the antenna wraps closely around the discharge chamber with the core around the antenna. A more detailed description is given in the following paragraphs. In this configuration, the magnetic flux paths have two portions, on inside the core and the other in the air/vacuum gap. For the sake of simplicity it is assumed there is no discharge chamber wall in the path here. The magnetic field strength H in the extended air gap, which is mainly responsible for plasma ignition and sustaining the discharge, is related to the magnetic field inside the core by[16]

$$H_{air} = \frac{\mu_{core}}{\mu_{air}} H_{core} \quad . \tag{1}$$

Selecting the core material is crucial for the application to minimize losses in the core. In our initial tests we used RF power at 144 MHz, but switched to the more common 13.56 MHz later on with the acquisition of a new RF power generator and automatic matchbox. A ferrite core possesses a complex relative permeability $\mu_r = \mu^{'} + i \cdot \mu^{''}$. The real part denotes the stored energy, whereas the imaginary part indicates the dissipation losses within the core.[25] The governing phenomena of this complex permeability for polycrystalline ferrites are domain wall motion and spin rotation magnetization.[25] The latter becomes dominant at frequencies of a few MHz.[25,26] This natural resonance has a limitation known as Snoek's limit

$$\mu^{'} f \approx 5600 \text{ MHz} \quad , \tag{2}$$

which limits the use of polycrystalline ferrites in RF applications.[25] This means that the maximum usable permeability decreases with frequency. Various core material blends from Fair-Rite were selected to test the influence of different real and imaginary ratios on the thruster and the discharge. Figure 2 shows the permeabilities of selected cores. Based on the $\mu^{'}/\mu^{''}$ ratios, both the FR-67 and FR-68 cores appear suitable for both 144 MHz and 13.56 MHz, while the FR-43 and FR-61 cores exhibit the characteristics of suppressor cores at these frequencies, especially at 144 MHz.

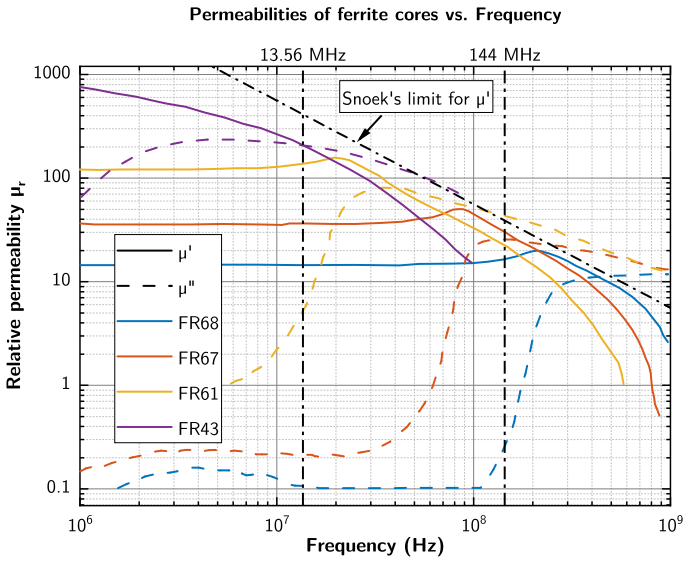

Figure 2: Complex permeabilities for different ferrite core material blends from Fair-Rite[27]

2. *Thruster design*

The thruster itself consists of a quartz glass discharge chamber for its high thermal durability, low permittivity and dielectric loss tangent, and very low secondary electron yield.[28–30] The antenna is surrounded by magnetic field generators that create the magnetic nozzle to increase the thrust beyond any thermal heating that occurs. The first prototype utilized two solenoids to easily change the magnetic field strength and test varying topologies. Based on the results, the iterated design now features permanent magnets. This more closely resembles an in-flight design, as it greatly reduces the power budget for the satellite. Figure 3 showcases both the initial prototype as well as the current design iteration. A more detailed description of the previous design is given by Peter et al.[31]

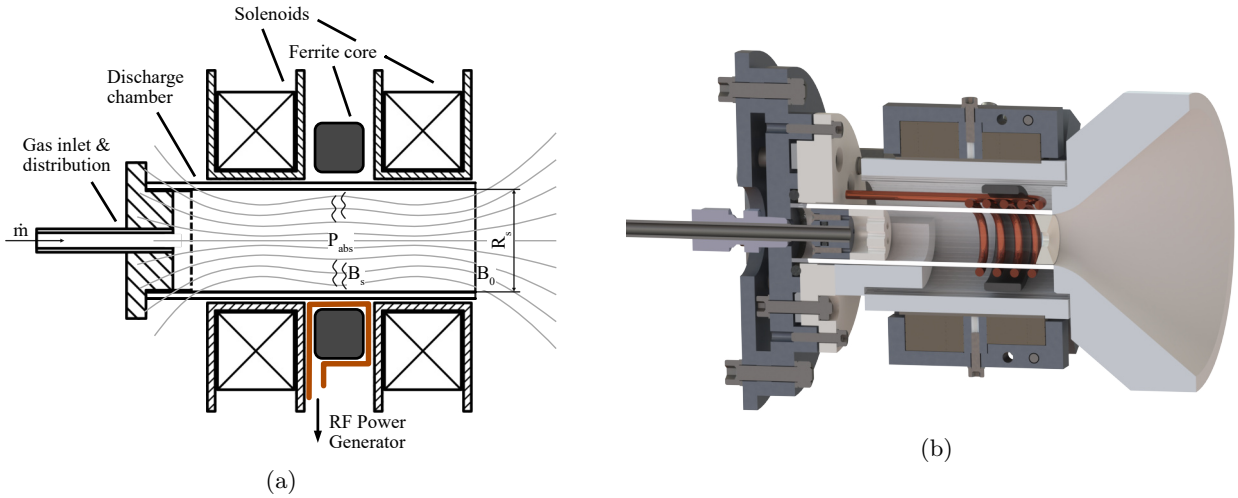

Figure 3: Illustration of the ferromagnetic enhanced ambipolar plasma thruster design: (a) Schematic of the initial prototype and (b) render of the current design iteration

To create the magnetic nozzle in the current design, stacks of permanent magnets are placed radially in a confining structure. The magnetic poles are orientated towards the discharge tube. This creates two distinct peaks along the thruster axis. One is located at the propellant feed shower head and the second downstream

at the ceramic aperture of the discharge tube. The aperture increases the neutral gas pressure inside the discharge chamber at low mass-flow rates. It was manufactured in-house from machinable alumina silicate ceramic due to its high thermal stability, very low coefficient of thermal expansion similar to quartz glass, and excellent vacuum compatibility. The magnetic field also features an inversion zone, where the antenna is located. This is meant to increase ion energy of the plume and the gradient in the magneto-static field in the antenna zone increases the RF coupling efficiency.[32] With this specific design it is also possible to test a quadrupole-like layout with very little modification. This will be studied in the upcoming month, as it might have a positive impact on focusing the plasma beam and decreasing the divergence of the plume. Attention was also given to the propellant feed to isolate any metal parts from the plasma potential with ceramic elements and make the shower head that distributes the gas more evenly inside the chamber movable along the thruster axis. This allows for tests on the effect of the exact position of the magnetic peaks with regards to the gas feed on thruster performance. The screen downstream of the discharge tube aperture aims to reduce the galvanic contact between the plasma and the grounded antenna.

C. Force Probe

The thrust is the most important performance parameter of any kind of thruster. For this, a reliable and well characterized thrust measurement system is fundamental for thruster development. The most common technique for thrust measurements is to place the thruster on a thrust balance with feedthroughs for power and propellant. This is quite challenging for RF thrusters because of the typically very ridged antenna structure, that also can not be connected easily through liquid metal contacts. It is possible to transfer the RF power onto a waveguide and transfer it across a small air gap. But this would require a highly customized thrust balance design. We wanted to utilize an existing high-precision thrust balance, that is both well characterized and already has a high technology readiness level due to multiple years of active in-house development.[33]

To use it with our RF thruster, or any kind of thruster system, that is difficult to mount on the balance, particle momentum instead of force acting on the thruster system is measured with a force probe design.[34,35] The force probe or collector is mounted in front of the double pendulum balance and collects incoming ions or fast particles in general in a way that it is unlikely that they exit the collector with significant velocity (see Fig. 4(a)). That way the collector absorbs all momentum from the particles, reducing the ambiguity about the amount of reflected and absorbed particles to a minimum. The collector is made from 0.5 mm titanium sheets because of its high strength to weight ratio compared to other metals, low thermal conductivity, and especially its low sputter yield. The collector is made of a 450 mm round base with 19 angled plates mounted on the surface, so that any impacting particle transfers its momentum to the collector through multiple reflections . The base is large enough to capture the whole particle beam of the thruster. The collector was initially designed with a shell to also capture the outermost reflected particles, but subsequent tests revealed that this was unnecessary and that removing it had a positive impact on the ambient pressure during testing.

To characterize the performance of the collector in terms of collection efficiency and measurement reliability compared to direct thrust measurements, a collector balance was tested in conjunction with an identical thrust balance and a Hall effect thruster with known characteristics mounted to it. The results of this initial study indicate that both measurement methods yield identical results, and that the collector force is 1:1 correspondent with the force experienced by the thruster.[33] The principle of this initial characterization of the collector is shown in Fig. 4(b). With the force probe setup, the thrust of our cathodeless thruster can easily be measured without having to determine it by means of plasma parameters or make assumptions regarding the electron energy distribution function. This also allows for efficient testing, as any change in thrust is visible immediately during testing. A description on the testing itself is given in Section III.

D. Plasma diagnostics

To get a more detailed insight into the operation conditions of the thruster at various factor settings, additional plasma diagnostics where developed. The focus was particularly on an E×B probe and an emissive probe. The emissive probe is used to determine the plasma potential, but it is much less sensitive to magnetic fields,[36] unlike a Langmuir probe, which is advantageous in conjunction with the static magnetic field of the thruster. The E×B probe can be used to determine the velocity distribution of the particle flow in order to gain a more

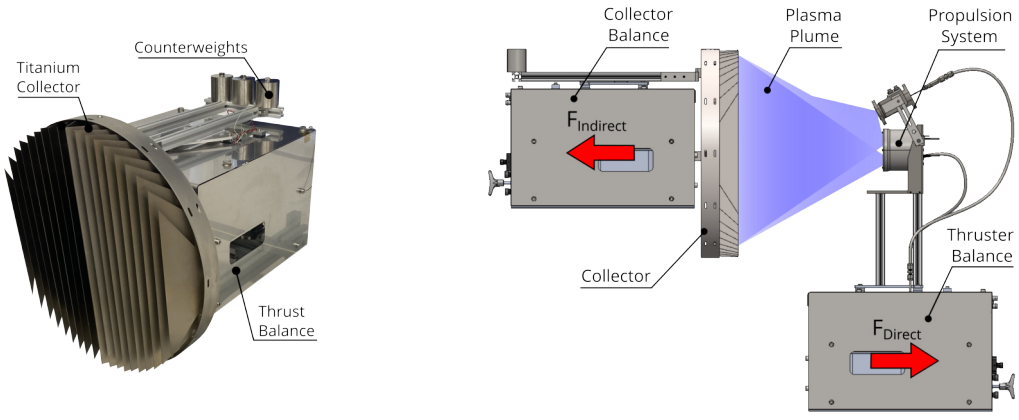

(a) (b)

Figure 4: (a) In-house developed compact thrust balance with force probe collector for thrust measurements and (b) working principle of force probe thrust measurements[33]

detailed insight into thrust generation and explain any shortcomings in efficiency. Both diagnostics where designed with rapid manufacturing in mind, so fused deposition modeling (FDM) was used wherever possible.

The E×B can also distinguish between multiply charged ions or several different species of ions, which might be the case with alternative propellants (see also Section E). In this case, the E×B probe works like as mass spectrometer, which is one of the reasons this was selected as a suitable diagnostic to design. The E×B probe was designed for velocities that can be expected with a magnetic nozzle acceleration, i.e. between $3\,\mathrm{km\,s^{-1}}$ to $15\,\mathrm{km\,s^{-1}}$. It uses stacks of six neodymium magnets at either side of the channel to generate a magnetic field as homogeneous as possible. The electric field is generated between two 1 mm copper sheets. Collimators both at the entrance and exit prevent particles not orthogonal to the magnetic and electric field lines as well as particles, that have been deflected inside the probe, from reaching the collector at the back. The front collimator is a quartz tube with 3 mm inner diameter and the one downstream can be varied by exchanging a stainless steel plate with an orifice, which currently also is 3 mm wide. To reduce any sputtering and secondary electron yield, a graphite target is used as a collector. Channels in the probe body allow particles, that reached the collector, to exit without letting particles enter from the outside. This was done to reduce the pressure at the back, which could otherwise have an influence on the measurement due to recombinations before reaching the target. Figure 5 (a) depicts the internal structure of the E×B probe.

The emissive probe is made from 0.5 mm tungsten wire crimped into 1 mm copper wire, which had a concentric hole drilled into one end. Both copper wires at either end of the tungsten wire are placed in separate quartz glass tubes for isolation and have connectors at the end. The tungsten wire forms an arch between the insulators. All parts are mechanically secured by a housing manufactured via FDM. Data acquisition of the floating potential is done between two $220\,\Omega$ resistors, following the recommended practice from Sheehan et al.[37] Additional metal sheets are used to shield the connectors at the an and the housing itself from RF radiation and plasma inside the vacuum chamber. Figure 5 (b) shows the emissive probe in its current state.

E. Alternative propellant storage system

In order to test other fuels in addition to krypton, argon, nitrogen and air as alternatives to xenon, a tank concept is presented below for operating the developed cathodeless thruster with these fuels. Solid propellants are of particular interest here, as they can be easily stored at a high storage density without the need for a pressurized tank. However, the propellant needs to be vaporized in this case. A low vaporization temperature and enthalpy are advantageous for this. Ideal fuels have a high density, high molecular mass, low ionization energy and are largely inert. There are already tank concepts based on bismuth[39] and iodine.[40] However, these have the disadvantage that bismuth has a comparatively high evaporation temperature and iodine is very reactive in combination with other substances and metals, which makes integration and operation

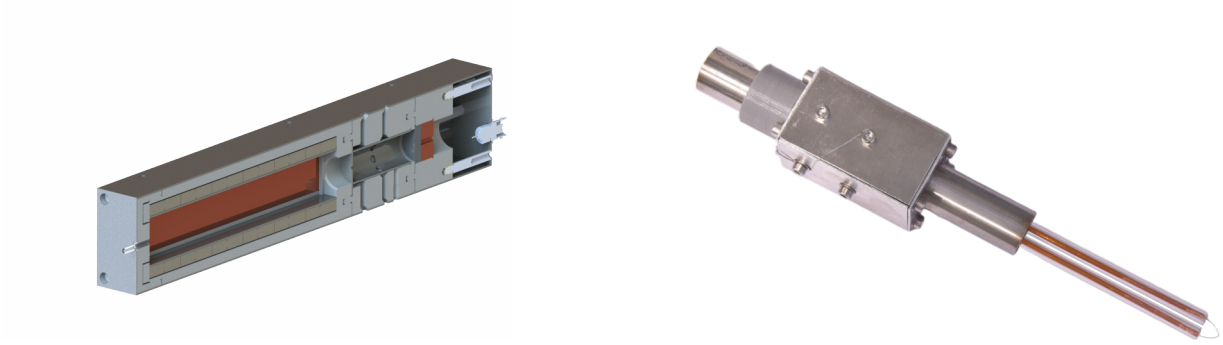

(a) (b)

Figure 5: (a) E×B probe and (b) Emissive probe in a hairpin design based on[37,38]

difficult. Based on the selection criteria, further potential fuel candidates can be found that are particularly interesting due to their high vapor pressure at low temperatures, i.e. that sublimate from the solid phase at low temperatures. The candidates summarized in Table 1 were determined on the basis of the data from.[41] The sublimation temperature is defined here as the temperature at which a vapor pressure of 100 Pa is reached. Some of the substances were ruled out from further evaluation and testing due to safety concerns. Adamantan, Camphor, and Naphthalene are considered in more detail due to their ready availability, low sublimation temperature, and low first ionization energy.

Table 1: Selection of potential propellant candidates based on the criteria presented with data from.[41] Candidates considered in more detail are shown in bold. The sublimation temperature is defined here as the temperature at which a vapor pressure of 100 Pa is reached.

Name	**Sublimation temperature** °C	**Melting point** °C	**Molecular mass** g/mol	**1st Ionization energy** eV
Adamantan	53.2	270.0	136.24	9.2
Acetamide	65.2	81	59.07	9.7
Camphor	41.5	179	152.23	8.76
Caprolactam	86.6	70	113.16	9.19
Hexamethylbenzene	81.7	156.6	162.28	7.85
Iodine	35.9	113.7	253.81	10.45
Naphthalene	49.3	80	128.17	8.12
Tetrabromomethane	25.6	90.1	331.63	7.5
Hexachloromethane	33.6	184	236.72	11.2

All of these substances are molecules. This is problematic for plasma formation, as many processes are possible that do not lead to ionization of the molecule, such as neutral dissociation. The energy used for this and similar processes can be regarded as a loss. The number of possible loss processes increases with the number of atoms in a molecular compound. A substance is therefore desired in which the ionization cross-section is as large as possible in comparison to the dissociation cross-section. As these values are not known for many molecules, another consideration is made based on mass spectrometry. The mass spectrograms of naphthalene, adamantane and camphor are shown in the appendix A. That of naphthalene shows a single high peak, from which it may be concluded that only a small amount of fragmentation occurs during ionization. Adamantane even has the special property that it has a higher dissociation energy than ionization energy due to its diamandoid structure.[42] Camphor was chosen as a comparison because it has a large number of peaks in the mass spectrum. It also has the lowest sublimation temperature. Both

adamantane and camphor have a great number of major peaks in their mass spectrograms, which is expected to have an influence on the ionization process. This can be tested in comparison to naphthalene.

The Hertz-Knudsen law establishes a relationship between the rate of sublimation into a vacuum and the vapor pressure, which is temperature-dependent.[43] If a tank system is vented to vacuum, the system pressure drops until the escaping mass flow is in equilibrium with the sublimation mass flow. This means that the propellant mass flow rate coming out of the tank system can be adjusted solely by the temperature. The vapor pressure can be easily determined for temperatures that do not approach zero using the empirical Antoine equation.[44] Antoine parameters are available in the literature for many substances, including the propellants selected here. Preliminary tests that were carried out also showed very good agreement between the vapor pressures determined as a function of temperature and the literature values.

In order to convert the substances into a gaseous state, a structure is required that can store the propellants and heat them as needed. It should also be easy to refill and handle for tests. As the substances recrystallize at lower temperatures than the sublimation temperature, the propellant channel up to the ionization chamber must be heated. A printed circuit board with a large number of vias was chosen for heating the propellant, as this represents a heating coil whose temperature can be determined comparatively accurately from the current characteristics and in which the holes are also heated due to the plating of the vias, which means that no or less propellant should get deposited in the holes. The circuit it designed to be operated at 5 V with a nominal power of 5 W. This will be sufficient to heat the upper layer of the propellant in vacuum to approximately 60 °C to 70 °C. A two-point controller is going to be used to control the mass-flow rate when the system is characterized.

A spring-piston mechanism is used to press the fuel against the heating plate and feed it as more and more fuel evaporates. The heating plate is connected through contacts that have been embedded into silicone to prevent leaks. This does not have to be vacuum tight, as the whole tank system will be placed inside the vacuum chamber. This makes the design simpler and less critical in the event of a leak. However the whole system has to be heated in order to prevent condensation. The objective of upcoming tests is to ascertain the mass flow rate of the various propellants that can be released continuously in accordance with the specified temperatures on the plate. This information can then be employed to regulate the mass flow through temperature control. Furthermore, the reaction time of the system to changes in the heating temperature is to be determined. Subsequently, the thruster will be operated with the selected propellants, and the performance will be compared with conventional propellants. Figure 6 shows the current design of the tank concept.

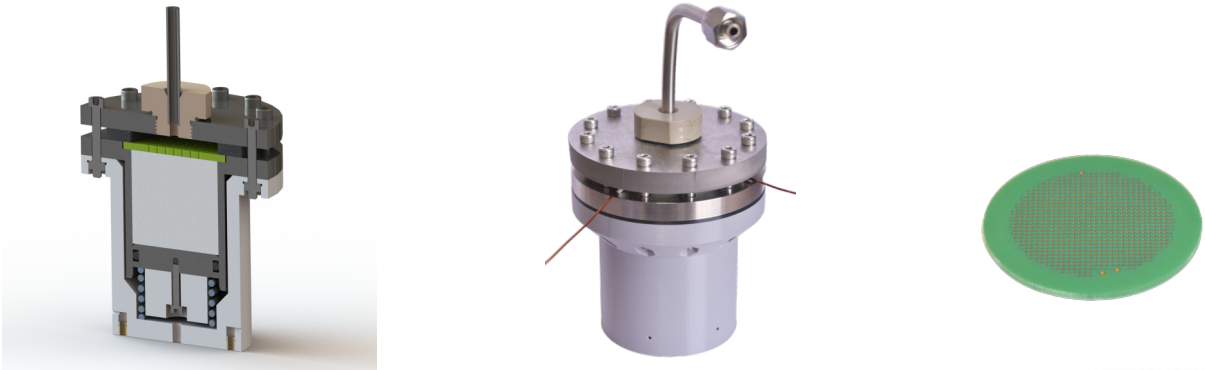

(a) (b) (c)

Figure 6: Tank design concept (a) render and (b) manufactured version for solid propellants with low sublimation temperature, as well as (c) the heater circuit board.

III. Tests and Results

A. Test setups

1. *Vacuum facilities*

All vacuum tests are performed in a 1 m long cylindrical vacuum chamber with an inner diameter of 0.5 m. The facility is equipped with an ECODRY 40 plus backing pump and a COOLVAC 10000 cryogenic pump from Leybold. The latter has a pumping capacity of $10\,000\,\mathrm{l\,s^{-1}}$ of nitrogen, achieving a base pressure of 5×10^{-8} mbar. All pumps, devices, and data acquisition systems are controlled by an in-house developed LabView based control software.

2. *RF power system*

The RF power system used for the tests presented here consists of an Advanced Energy® CESAR 1310 RF generator with 1 kW of maximum output power and a compatible automatic NAVIO matchbox, also from Advanced Energy® . The system operates at 13.56 MHz. The previous RF power system with a self-build matchbox was operated at 144 MHz.[31] However, due to power constraints, we have opted to transition to the new system. In addition, automatic matching during operation is possible with the current setup.

B. Magnetic field measurements

1. *Thruster*

Samarium-cobalt permanent magnets are used as magnetic generators in the current design. To measure the magnetic flux density inside the discharge channel as well as downstream of the thruster exit and compare it to the analysis, a TLE493D Hall effect sensor was moved through the assembly on a CNC table. The analysis during the design phase was done with FEMM. Figure 7 shows both a slice through the central axis of the thruster and a comparison between analysis and measurement on the thruster axis. As the FEMM simulation is only two-dimensional with rotational symmetry, the magnet stacks had to be simulated as ring magnets. This naturally results in an estimation error, as more magnet material is assumed than is actually present. However, if the volume of the simulated ring magnet is set in relation to the real volume of the arranged blocks of magnets, a correction factor is obtained with which the actual magnetic flux density can be estimated much better. Of course, this is also only an approximation, but it is useful for initial designs before measurements can be performed. In Fig. 7 (b), a very good agreement can be seen between the measurement and the simulation results, which were corrected with this factor. One reason for the good agreement could also be the small height of the magnet stacks compared to their radius.

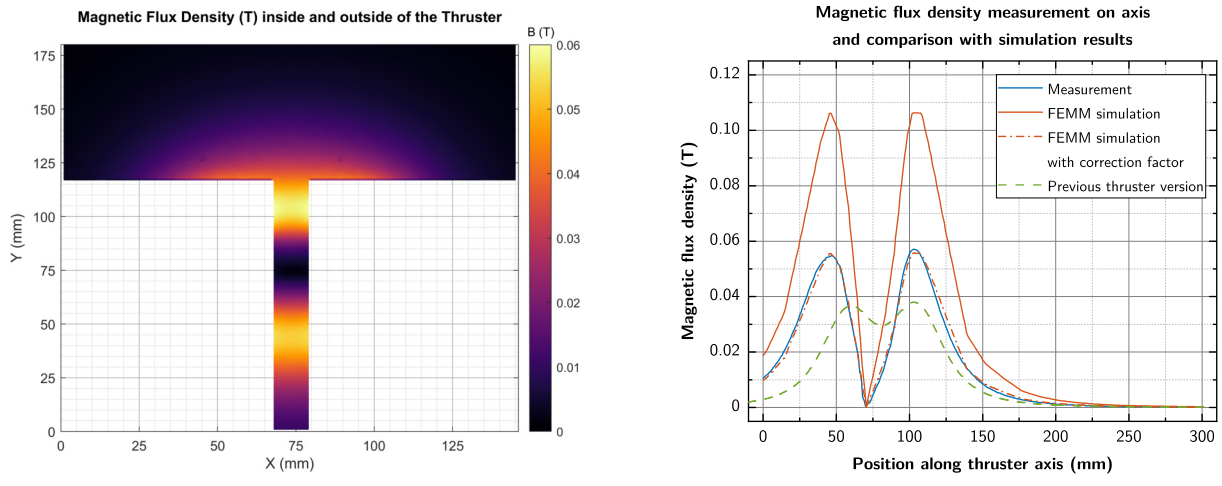

(a) (b)

Figure 7: Magnetic flux density (a) in the plane through the central axis of the thruster and (b) one dimensional on the central axis

Although the magnetic flux density of the current design is considerably less than with a comparable ring magnet design, the latter would have required custom made magnets, which are both costly and have long lead times. Nevertheless, the flux density is about 50 % higher than with the previous solenoidal design. The magnetic flux density of the previous thruster design is also included in Fig. 7 (b). And if significant improvements in performance compared to the previous design are attributed to the magnetic field, there is still the option to manufacture ring magnets, which would result in a higher overall magnetic flux density. With the current design, the magnetic field strength can also be adjusted slightly by adding individual cuboid magnets to the magnet stacks. A quadrupole arrangement can also be tested, which could help to further focus the plasma beam.

2. E×B probe

The magnetic flux density of the ExB probe was also measured. Inside of the channel it is very uniform at 0.1233 T with a deviation of ±0.68 mT in a zone of 4x4 mm around the axis with a relatively steep gradient at the channel exit. Figure 8 shows the measured data on the central axis superimposed with an image of the probe.

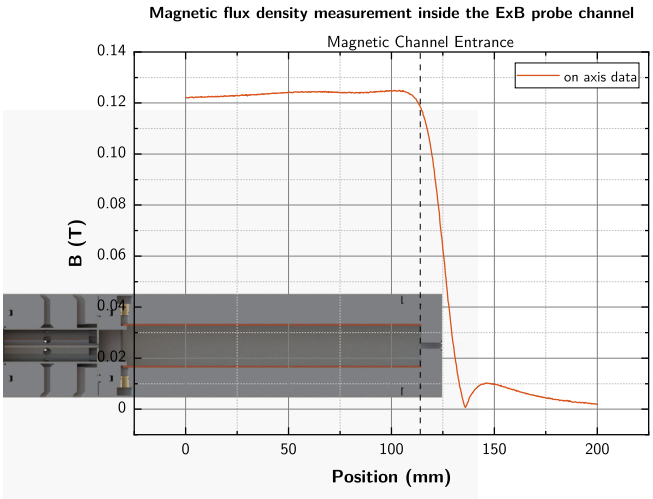

Figure 8: Magnetic flux density measurement inside the E×B probe channel

C. Thruster testing

While at the beginning of the project the diagnostic of the thruster was mostly optical,[31] as the other diagnostics still had to be developed, tests in the current iteration mainly consist of thrust measurements with the particle momentum measurement setup described in Section II. That's because thrust is one of the most important metrics of any thruster and other performance parameters can also be calculated from it without ambiguity. The total thrust f_T of an electric propulsion system consists of the cold gas thrust f_G and the additional plasma thrust f_P

$$f_T = f_G + f_P \tag{3}$$

that is generated by means of whatever acceleration mechanism the thruster uses. To avoid error from drifts during the duration of the test, both components are determined separately. The cold gas thrust is calibrated for the mass flow levels to be tested at the beginning and at the end of each test multiple times. The relationship between the cold gas flow and the thrust force is always linear within the tested mass flows, which is to be expected for a simple expansion into vacuum without a special nozzle. After ignition, the plasma thrust is determined for all operating points or factor settings for this test. A measurement point always consists of cold gas level, ignition, reaching stable operation and waiting for the balance to stabilize, and thruster shutdown. The difference between the cold gas level and the stable level during ignition is the

plasma thrust. This is done multiple times to increase the confidence in the measurement. At the time, argon, krypton, nitrogen, and air have been tested with the current design in this manner.

One goal of the first prototype was to test different core materials and their influence on operation and performance. To this end, the core materials described in Section II Subsection B were tested in different antenna arrangements. These are shown in Fig. 9.

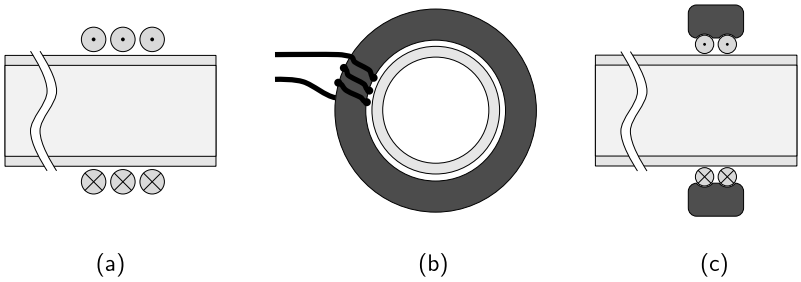

Figure 9: Different antenna and core configurations that have been tested. (a) Standard loop antenna with different loop counts, (b) concentric ferrite core with antenna around the core, and (c) loop antenna with concentric ferrite core.

Variant (b) was discarded after a short time, as the core becomes very hot during testing and stable ignition could not be achieved with the current 13.56 MHz RF power system. Using 144 MHz, however, operation with this configuration was possible.[31] Due to very poor performance after switching to the current 13.56 MHz system with the 1 mm antennas used up to that point, the antenna thickness was also varied, with 3 mm found to be the sweet spot between manufacturing the antenna and operation.

It was found that the FR-43 and FR-61 core materials indeed act as suppressors (see Section II and Fig. 2). No ignition could be achieved with the FR-43, and the system with the FR-61 core performed significantly worse compared to a plain loop antenna. However, the other two cores tested, FR-67 and FR-68, showed a significant improvement in ignitability and a significantly lower power at which a measurable thrust is achieved. This point of power increase, where a clear change in operating mode can be observed, accompanied by a clearly measurable thrust signal, is associated with the transition between capacitively coupled and inductively coupled modes of the antenna.

Nevertheless, very poor performance was observed with the first version of the thruster and no stable transition to the inductive mode could be achieved. For this reason, tests were also carried out with different aperture configurations in order increase the neutral gas pressure in the discharge tube, even at lower mass-flow rates, to achieve a stable inductive discharge. The tested apertures are shown in Fig. 10.

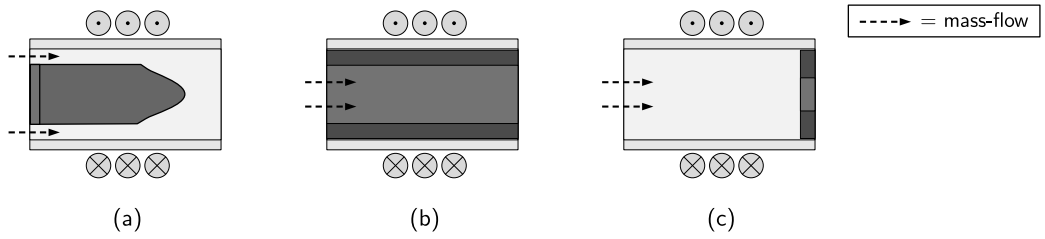

Figure 10: Different aperture variants that have been tested.

The idea behind (a) was to direct the mass flow closer under the antenna. Unfortunately, no ignition was achieved, so no further tests were carried out with it. The goal of (b) was to test a smaller discharge tube without having to change the rest of the design. Although reliable ignition was achieved, the discharge was only very weak compared to the test without the concentric cylinder, which is probably due to the greater distance to the antenna's magnetic field. In contrast, variant (c) showed a significant improvement in the operating state and ignition at low mass flows. The transition to the inductive mode thus takes place at

lower RF power and mass-flow rates and the plasma has a higher energy overall. For this reason, this form of aperture is used in all further tests and also incorporated into the current design. Due to the now higher temperatures of the plasma, the aperture initially made from polyether ether ketone (PEEK) also had to be replaced by ceramic. Please note, that descriptions of tests with different variants of core materials, antenna configurations, and apertures have been sorted by category in the description given here, not in chronological order, to present everything in a more structured way. The findings are compiled from a number of different tests.

With a 2 mm antenna and a 10 mm aperture, an inductively coupled mode generating additional thrust was achieved for the first time, both with a standard loop antenna and a core configuration similar to Fig. 9 (c). Later improvements involved further increasing the antenna diameter to 3 mm and adjusting the aperture diameter to 5 mm. It was observed that by adding the core to the antenna, the power required to reach an operating state that provides additional plasma thrust, i.e. the inductively coupled mode, was almost halved for both argon and krypton, going down to 200 W and 100 W, respectively for the first prototype. Regardless of the improvements made, performance was still very poor with the thrust ranging from 534 µN to 1020 µN at 150 W to 600 W RF power and 0.374 mg s^{-1} to 0.623 mg s^{-1} of krypton. The resulting I_{sp} is about 98 s to 291 s and the thrust efficiency below 1 % across all measurements. However, advantages of the antenna core have already been observed in terms of performance. This is the basis for the design iteration presented in Fig. 3 (b), which incorporates all of the findings described above.

The chamber diameter was subsequently reduced to 17 mm with a ceramic aperture of 5 mm diameter to further increase the neutral gas pressure and improve the mode jump. The aperture was incorporated directly into the design and the general aim was to achieve a more integrated design with more heat-resistant ceramic parts, as the antenna gets fairly hot during testing. As described above, the solenoids from the first prototype where also exchanged for two rings of permanent magnet stacks, that create two distinct peaks along the central axis with a magnetic indentation zone between them. The maximum magnetic flux density is also increased from 38 mT to 57 mT. The loop count of the antenna was also increased to 4 with a 3 mm wire. As a result, a significant reduction in the mass flow required for a stable inductively coupled operation was observed from the very first ignition. The power required for the mode jump was also reduced from 150 W to less than 50 W, down to 20 W to 30 W. Figure 11 shows the current thruster version before and during thrust measurements.

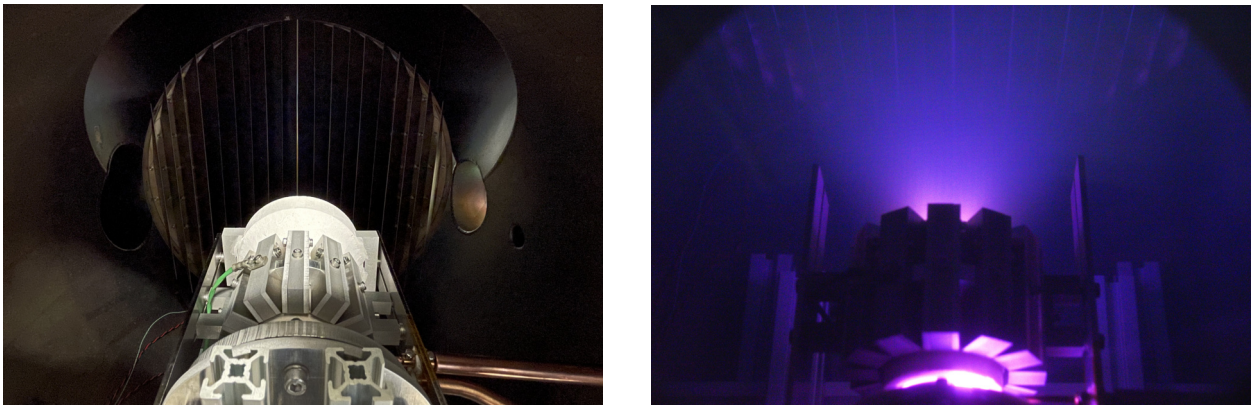

(a) (b)

Figure 11: Current iteration of the cathodeless thruster (a) in thrust measurement test setup and (b) during testing.

Figure 12 shows an exemplary thrust measurement sequence for both krypton and argon. Note the high ratio of reflected to forward RF power at the beginning of the sequence in Fig. 12 (b). This is because the system was matched to the inductive mode, but the mode transition has not taken place. At a threshold input power the mode switches and the reflective power decreases abruptly. This must also be taken into account when the thruster is initially ignited. Therefore, a small discharge of a few watts is always maintained during

the thrust measurements between the thrust periods. This does not generate a measurable plasma thrust but simplifies the transition to the inductive mode, as a small number of free charges remains present.

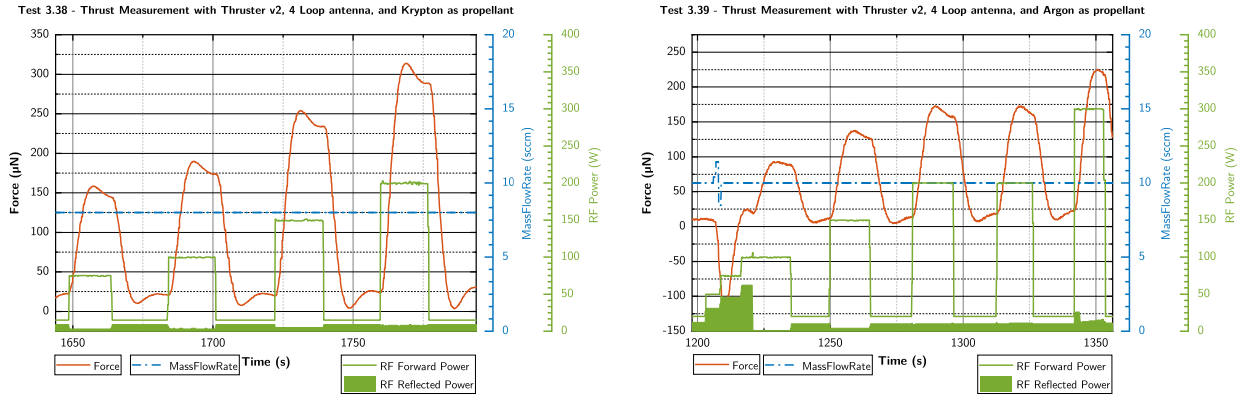

(a) (b)

Figure 12: Section of a thrust measurement sequence for (a) krypton and (b) argon. The trend in the thrust has been removed in post processing to make data analysis easier, as the balance experiences a slight linear drift over the cause of the measurements. However, this can be neglected for the evaluation of the thrust because, as described, the plasma thrust is determined individually for each thrust sequence and added to the calibrated cold gas thrust.

Summarized performance data for the comparison between an antenna without a ferrite core and an antenna with a ferrite core are shown in Table 2. No significant difference was found between the FR-67 and FR-68 cores in the tests performed so far. In each case, the lower power required to reach the mode transition was clearly evident. Of course, this also improves the force per watt of electrical power. In addition, ignition at power levels below 50 W was only possible when using a ferrite core. However, it can also be seen that the I_{sp} actually decreased slightly when using an antenna core. One reason for this could be the small fraction of power that is dissipated inside the core and therefore does not contribute to plasma generation and heating.

Table 2: Summary of the performance for all tests carried out with the described current thruster system and with different propellants. The individual columns show the range measured. The low and high values do not necessarily belong to the same operating point, but a clear trend is observed were increasing the input power increases both the thrust and I_{sp}, which is expected. The efficiency is calculated by dividing the total force by the input RF power.

Description		**Thrust**		**Input Power**		**Efficiency**		**I_{SP}**		**Mass-flow**	
		µN		W		µN/W		s		mg/s	
Loop antenna	Krypton	115	770.3	56	487	1.03	12.01	105.5	364.2	0.093	0.498
	Argon	88.1	643.1	82	472	0.56	3.60	136.7	517.2	0.059	0.237
	Air	65.5	395.5	91	481	0.36	1.88	144.5	352.6	0.042	0.208
Antenna + FR-67 core	Krypton	87.5	1432.2	15	370	1.11	64.4	95.51	248.6	0.125	0.935
	Argon	80.0	700.9	30	424	1.47	7.19	135.8	400.1	0.059	0.297
	Air	51.1	1128.9	49	462	1.33	14.42	119.6	233.4	0.042	0.625

It was also observed that the second peak of the magnetic field should indeed coincide with the narrowest cross-section of the aperture, as described by Trezzolani et al.,[32] as otherwise the performance and operating behavior is significantly worse. This was observed in a test in which the aperture was too far downstream, i.e.

the peak of the magnetic field was still in front of the aperture for the plasma. Furthermore, an aperture reduced to 3 mm was tested, but this also resulted in a decreased performance. A test with a slightly larger aperture for comparison is still pending. The current thruster version has notches in the ferrite core so that the antenna is enclosed further by the core and is closer to the quartz glass. The described effects were observed for all of the tested propellants. Figure 13 shows the thruster operating on argon and air. Tests with the emissive probe and the E×B probe have not yet been carried out, but are planned for the coming weeks.

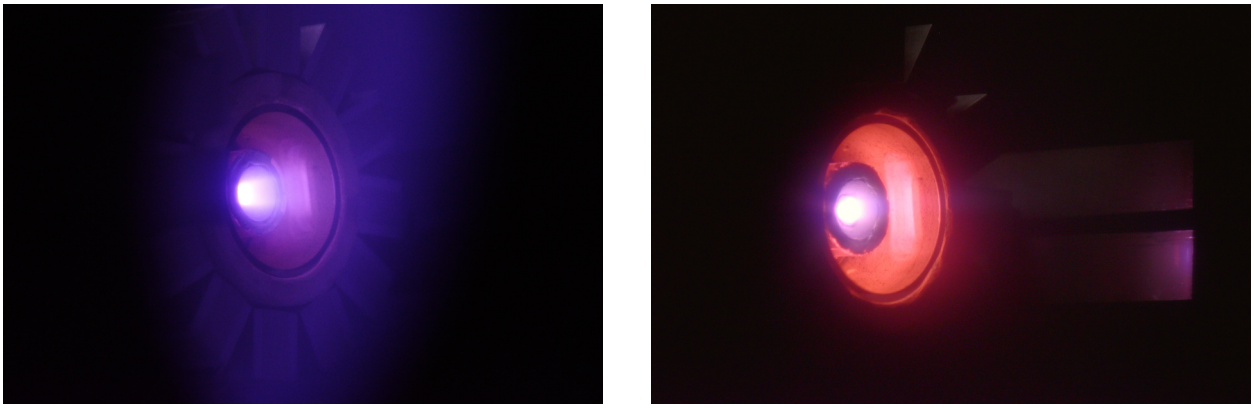

(a) (b)

Figure 13: Thruster operating on (a) argon and (b) air

IV. Conclusion

The tests conducted provided a great deal of information about the first thruster prototype, which has been incorporated into the successor design presented here. At the end of last year, no measurable thrust could be determined with the thruster, while reliable ignition and transition to thrust mode is now possible at less than 50 W with various propellants. The current system is much more compact than the first test model and requires only the RF input line due to the permanent magnets. This brings it one step closer to a fully integrated system for use on a small satellite. However, the performance expected at the beginning of the design has not yet been achieved. The thrust efficiency is still below 2 % and the I_{sp} values are not yet comparable to similar systems in the same power class. Determining the reasons for the poor performance and improving it is one of the main goals of further development.

Tests with the designed E×B and emissive probes are pending. The influence of the magnetic field topology on the performance will be further investigated by testing the modified position of the gas inlet with respect to the first magnetic field peak in the thruster. In addition, other aperture diameters and their influence on thruster operation will be tested. It may also be advantageous to transfer the thruster and thrust balance to our largest vacuum facility. The additional pumping speed achieves a lower pressure during operation, which can have a huge impact on the performance of an RF thruster.[45]

The thrust measurement setup built in conjunction with the presented activity was particularly successful. Using the particle momentum balance, the performance of the thruster system can be determined directly and without uncertainty about the assumptions to be made. The direct feedback of changes in thrust for different factor settings allows rapid iterations.

As part of the investigation of alternative propellants suitable for use with the developed RF thruster, a tank system that sublimates solid propellants has been developed. The vapor pressure curves of selected propellants have already been determined, so the next step is to characterize the mass flow of the tank system before conducting initial ignition tests with the thruster. The solid propellants under investigation represent an interesting alternative to conventional gases, especially for small satellites, provided they offer comparable performance. These tests are also planned for the coming months.

Appendix

A. Mass spectrograms of selected alternative propellants

The following Fig. 14 shows the mass spectrograms of the three selected alternative solid propellants described in Section II Subsection E.

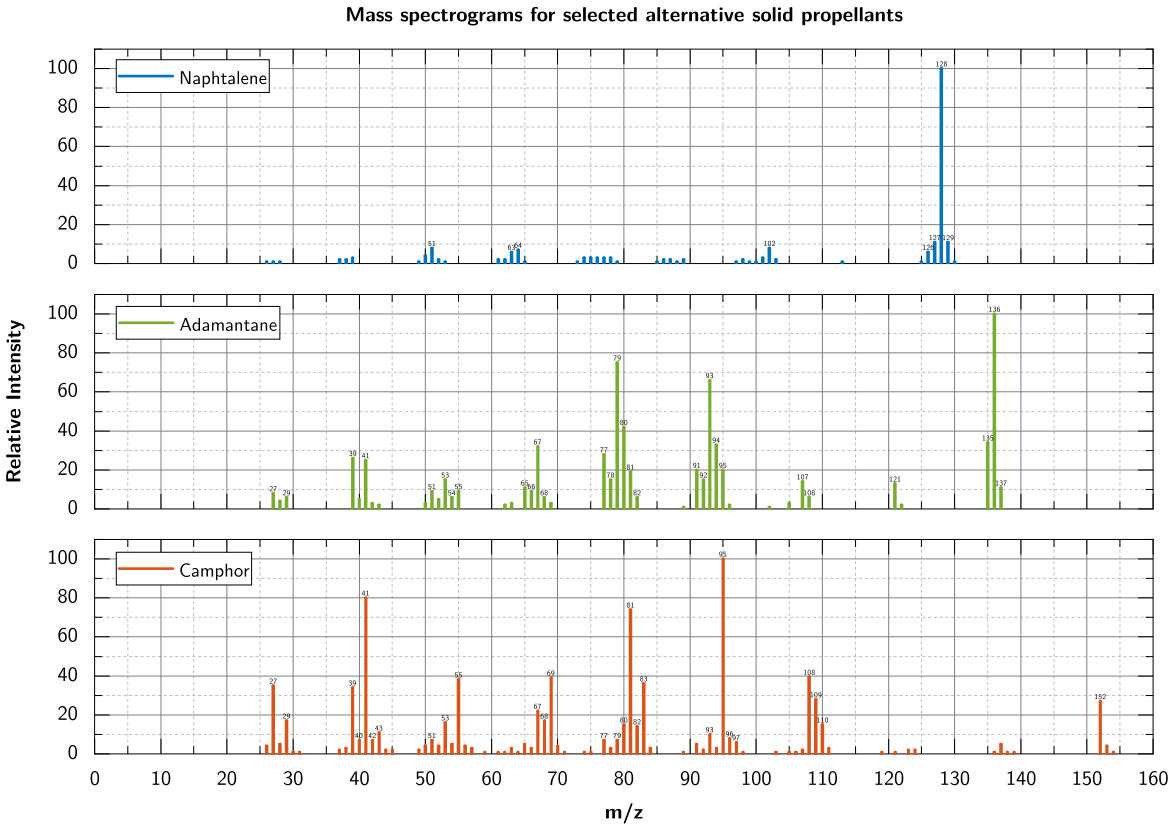

Figure 14: Mass spectrograms of selected alternative propellants. Data taken from the National Institute of Standards and Technology (NIST) website.[46]

Acknowledgments

The authors gratefully acknowledge funding by the German Aerospace Center DLR (50RS2103).

References

[1]J. M. Urrutia and R. L. Stenzel, "Helicon modes in uniform plasmas. i. low m modes," *Physics of Plasmas*, vol. 22, no. 9, p. 092111, 2015.

[2]R. L. Stenzel and J. M. Urrutia, "Helicon modes in uniform plasmas. iii. angular momentum," *Physics of Plasmas*, vol. 22, no. 9, p. 092113, 2015.

[3]R. L. Stenzel and J. M. Urrutia, "Helicon waves in uniform plasmas. ii. high m numbers," *Physics of Plasmas*, vol. 22, no. 9, p. 092112, 2015.

[4]S. Shinohara, Y. Miyauchi, and Y. Kawai, "Dynamic plasma behaviour excited by m=+or-1 helicon wave," *Plasma Physics and Controlled Fusion*, vol. 37, no. 9, pp. 1015–1030, 1995.

[5]S. Shinohara, H. Nishida, T. Tanikawa, T. Hada, I. Funaki, and K. P. Shamrai, "Development of electrodeless plasma thrusters with high-density helicon plasma sources," *IEEE Transactions on Plasma Science*, vol. 42, no. 5, pp. 1245–1254, 2014.

[6]J. P. Sheehan, B. W. Longmier, I. Reese, and T. Collard, "New low-power plasma thruster for nanosatellites," in *50th*

AIAA/ASME/SAE/ASEE Joint Propulsion Conference: JPCE, (Reston, Virginia), American Institute of Aeronautics and Astronautics, 2014.

[7]U. M. Siddiqui, C. Cretel, J. Synowiec, A. G. Hsu, J. a. Young, and R. Spektor, "First performance measurement of the phase four rf thruster," in *35th International Electric Propulsion Conference: IEPC*, (Reston, Virginia), American Institute of Aeronautics and Astronautics, 2017.

[8]T. Furukawa, K. Takizawa, D. Kuwahara, and S. Shinohara, "Electrodeless plasma acceleration system using rotating magnetic field method," *AIP Advances*, vol. 7, no. 11, p. 115204, 2017.

[9]P. Smirnov, R. Kozakov, and J. Schein, "Experimental characterization of the capacitively coupled rf-plasma thruster," *Applied Sciences*, vol. 11, no. 15, p. 6799, 2021.

[10]F. Filleul, A. Caldarelli, C. Charles, R. W. Boswell, N. Rattenbury, and J. Cater, "Characterization of a new variable magnetic field linear plasma device," *Physics of Plasmas*, vol. 28, no. 12, 2021.

[11]J. Eugene, *Empirical Aspects of a Mini-Helicon Plasma Thruster Experiment*. Dissertation, Massachusetts Institute of Technology, 2006.

[12]V. Godyak, "On helicon thrusters: Will they ever fly?," *Journal of Applied Physics*, vol. 127, no. 10, p. 103301, 2020.

[13]V. Godyak, "Inductive plasma source with high coupling efficiency," 2014.

[14]V. A. Godyak, "Electrical and plasma parameters of icp with high coupling efficiency," *Plasma Sources Science and Technology*, vol. 20, no. 2, p. 025004, 2011.

[15]V. Godyak, "Ferromagnetic enhanced inductive plasma sources," *Journal of Physics D: Applied Physics*, vol. 46, no. 28, p. 283001, 2013.

[16]S. Lloyd, D. M. Shaw, M. Watanabe, and G. J. Collins, "Ferrite core effects in a 13.56 mhz inductively coupled plasma," *Japanese Journal of Applied Physics*, vol. 38, no. 7S, p. 4275, 1999.

[17]L. R. Nerone and A. H. Qureshi, "Mathematical modeling and optimization of the electrodeless, low-pressure, discharge system," *Proceedings of IEEE Power Electronics Specialist Conference*, pp. 509–514, 1993.

[18]G. Lister, J. Lawler, W. Lapatovich, and V. Godyak, "The physics of discharge lamps," *Reviews of Modern Physics*, vol. 76, no. 2, pp. 541–598, 2004.

[19]G. Leray, *PEGASES: Plasma Propulsion with Electronegative Gases*. Dissertation, École Polytechnique, Paris, 2009.

[20]D. Renaud, S. Mazouffre, and A. Aanesland, "Plasma composition and ion acceleration in the pegases thruster," in *Space Propulsion - 2014: SP*, 2014.

[21]D. Renaud, S. Mazouffre, and E. Pawelec, "Investigation of the pegases thruster magnetic filter via laser photodetachment experiments," in *34th International Electric Propulsion Conference: IEPC*, (Reston, Virginia), American Institute of Aeronautics and Astronautics, 2015.

[22]D. Rafalskyi and A. Aanesland, "Plasma acceleration using a radio frequency self-bias effect," *Physics of Plasmas*, vol. 22, no. 6, p. 063502, 2015.

[23]M. Celik and H. Kurt, "Ferromagnetic enhanced inductively coupled plasma cathode for thruster ion neutralization," in *17th International Conference on Ion Sources: ICIS*, AIP Conference Proceedings, p. 090022, 2018.

[24]V. Godyak, Y. Raitses, and N. J. Fisch, "Rf plasma cathode-neutralizer for space applications," in *30th International Electric Propulsion Conference: IEPC*, (Reston, Virginia), American Institute of Aeronautics and Astronautics, 2007.

[25]Y.-K. Hong and J. Lee, "Ferrites for rf passive devices," in *Recent Advances in Magnetic Insulators – From Spintronics to Microwave Applications*, vol. 64 of *Solid State Physics*, pp. 237–329, Elsevier, 2013.

[26]T. Nakamura, "Snoek's limit in high-frequency permeability of polycrystalline ni–zn, mg–zn, and ni–zn–cu spinel ferrites," *Journal of Applied Physics*, vol. 88, no. 1, pp. 348–353, 2000.

[27]Fair-Rite, "Ferrite components for the electronics industry," 2013.

[28]Heraeus Quarzglas GmbH & Co. KG, "Quarzglas für optische anwendungen: Daten und eigenschaften," 2023.

[29]WISAG AG, "Quarzglas für die optik: Technische eigenschaften."

[30]A. Dunaevsky, Y. Raitses, and N. J. Fisch, "Secondary electron emission from dielectric materials of a hall thruster with segmented electrodes," *Physics of Plasmas*, vol. 10, no. 6, pp. 2574–2577, 2003.

[31]C. Peter and M. Tajmar, "Development of a novel ambipolar plasma thruster for nanosatellites and air breathing applications," in *74th International Astronautical Congress: IAC*, 2023.

[32]F. Trezzolani, A. L. Fabris, D. Pavarin, A. Selmo, A. I. Tsaglov, A. V. Loyan, O. P. Rubalov, and M. Manente, "Low power radio-frequency plasma thruster development and testing," in *33rd International Electric Propulsion Conference: IEPC*, (Washington, DC), American Institute of Aeronautics and Astronautics, 2013.

[33]O. Neunzig and M. Tajmar, "Verification of a novel collector-thrust measurement using low-power hall-effect thruster," in *9th Space Propulsion Conference: SP*, 2024.

[34]A. Spethmann, T. Trottenberg, H. Kersten, F. G. Hey, L. Grimaud, S. Mazouffre, D. Bock, and M. Tajmar, "Force probes for development and testing of different electric propulsion systems," *EPJ Techniques and Instrumentation*, vol. 9, no. 1, 2022.

[35]Seshan and Krishna, *Handbook of thin film deposition: Techniques, processes, and technologies*. Waltham, Mass. and Amsterdam and Heidelberg: William Andrew and Elsevier, 3. ed. ed., 2012.

[36]J. D. Gerst, *Investigation of magnetized radio frequency plasma sources for electric space propulsion*. Dissertation, Université d'Orléans, Orléans, 2014.

[37]J. P. Sheehan, Y. Raitses, N. Hershkowitz, and M. McDonald, "Recommended practice for use of emissive probes in electric propulsion testing," in *33rd International Electric Propulsion Conference: IEPC*, (Washington, DC), American Institute of Aeronautics and Astronautics, 2013.

[38]J. P. Sheehan and N. Hershkowitz, "Emissive probes," *Plasma Sources Science and Technology*, vol. 20, no. 6, p. 063001, 2011.

[39]A. Sengupta, C. Marrese-Reading, A. Semenkin, L. Zakharenkov, S. Tverdokhlebov, O. Tverdokhlebov, K. Polzin, T. Markusic, M. Capelli, D. Scharfe, I. Boyd, M. Keidar, A. Yalin, and V. Surla, "Summary of the vhital thruster technology demonstration

program: A two-stage bismuth-fed very high specific impulse tal," in *30th International Electric Propulsion Conference: IEPC*, (Reston, Virginia), American Institute of Aeronautics and Astronautics, 2007.

[40]D. Rafalskyi, J. M. Martínez, L. Habl, E. Zorzoli Rossi, P. Proynov, A. Boré, T. Baret, A. Poyet, T. Lafleur, S. Dudin, and A. Aanesland, "In-orbit demonstration of an iodine electric propulsion system," *Nature*, vol. 599, no. 7885, pp. 411–415, 2021.

[41]J. Speight, *Lange's Handbook of Chemistry, Seventeenth Edition*. New York, N.Y.: McGraw-Hill Education and McGraw Hill, 17th edition ed., 2016.

[42]P. Dietz, *Charakterisierung molekularer Treibstoffe für den Einsatz in Hochfrequenz-Ionentriebwerken*. Dissertation, Justus-Liebig-Universität Gießen, Gießen, Germany, 2023.

[43]A. H. Persad and C. A. Ward, "Expressions for the evaporation and condensation coefficients in the hertz-knudsen relation," *Chemical reviews*, vol. 116, no. 14, pp. 7727–7767, 2016.

[44]N. Schörghofer and J.-P. Williams, "Sublimation pressures of common volatiles at low temperature and maps of supervolatile cold traps on the moon," *Icarus*, vol. 416, p. 116086, 2024.

[45]T. Vialis, J. Jarrige, and D. Packan, "Geometry optimization and effect of gas propellant in an electron cyclotron resonance plasma thruster," in *35th International Electric Propulsion Conference: IEPC*, (Reston, Virginia), American Institute of Aeronautics and Astronautics, 2017.

[46]NIST, "Nist chemistry webbook," 2023.